The Invagination of Excess Surface Area by Shrinking Neurons

C. E. Morris,* J. A. Wang,* and V. S. Markin†
*Neuroscience, Ottawa Health Research Institute, Ottawa Hospital, Ottawa, Ontario, Canada; and †Department of Anesthesiology/Pain Management, University of Texas Southwestern Medical Center, Dallas, Texas

ABSTRACT Over most of their surface, neurons are surrounded by a narrow extracellular gap across which they make adhesive cell-cell contacts. Thus constrained, how do they regulate their geometry when osmotically perturbed? Specifically, are there any interesting consequences of local osmosis in such conditions? Using confocal imaging of shrinking neurons in culture, we observe water exiting into the cell-substratum gap. This water efflux generates a hydrostatic pressure that, at discrete (low adhesion) sites, causes the neuron's excess plasma membrane to invaginate, thus compensating for shrinkage with a pseudo-intracellular volume. To identify the minimal requirements of the process, a compartment/flux model was constructed. It comprises, essentially, a large liposome adhering in a labyrinthine fashion to a substratum. The model predicts that invaginations form at the cell-substratum interface under the influence of local osmosis, provided that adhesion across the gap is neither too tight nor too loose. Local osmosis in the central nervous system, in contrast to epithelia, is usually considered a mishap, not a physiological opportunity. We postulate, however, that local osmotic forces acting in conjunction with confined extracellular spaces could be harnessed in service of surface area, shape, and volume regulation when intense neural activity alters a neuron's osmotic balance.

INTRODUCTION

Over most of their surface, neurons adhere to other neurons and to glia (e.g., see Chklovskii et al., 2002, and references therein). Surrounding them is a tortuous extracellular compartment that is small compared to the cellular compartment. Given this tissue geometry, osmotic shrinkage in a neuron will entail consequences not experienced by cells in suspension. In practical terms, cell shape and volume changes in central nervous system (CNS) cells have implications for volume transmission, drug delivery, and intra- and intercellular signaling (Nicholson et al., 2000). A partial list of responses of isolated neurons to anisosmotic media includes: regulatory volume changes, no detectable volume change, volume-induced changes of membrane area (equals capacitance), and membrane tension (tether force), and changes in outgrowth patterns (Aitken et al., 1998; Pasantes-Morales et al., 2000; Wan et al., 1995; Dai et al., 1998; Bray et al., 1991). Of particular interest here is the fact that from mollusks to mammals, central neurons respond to abrupt hyperosmotic stimuli not simply by shrinking, but by inflating collections of pseudo-intracellular spaces (vacuole-like dilations or VLDs) as they shrink (Morris and Homann, 2001). During these dynamic events, neurons are remarkably effective at preserving, in detail, their adhesive contacts. To the extent that the shrinking cytoplasmic volume is compensated by the dilating invaginations, this would damp cell shape changes and preserve cell-cell contacts. In effect, it should contribute to a concerted regulation of neuronal volume, surface area, and shape, thereby sparing the CNS's synaptic cyto-architecture (Morris, 2001a). In this regard, it is interesting that after exposure to extreme hypotonic or hypertonic stress, hippocampal CA1 recordings demonstrate that on return to isotonic solution, neurons retain their ability to generate synaptic responses (Tao, 1999). Dendrites are of special interest since the minute volume of dendritic spines and their intense ion fluxes engender large osmotic excursions. Whether excess membrane invaginates along dendritic shafts (see Cooney et al., 2002) during swell-shrink episodes has not, however, been investigated. It is known that transmitter-stimulated Na influx causes reversible dendritic swelling attended by internalization of membranous receptors (Ikegaya et al., 2001) but whether the latter represents membrane invaginated as a part of regulatory shrinkage (see Czekay et al., 1994; Morris, 2001a) is unknown. In terms of neuronal subregions, it is known that discrete shrinkage-induced membrane invaginations develop at the adherent surfaces of growth cones, neuritic processes, and somata (Reuzeau et al., 1995); such invaginations have also been observed for hippocampal glial cells L. R. Mills and C. E. Morris (unpublished observation). In addition to CNS cells, the dilation of pseudo-intracellular spaces in shrinking cells has been examined in skeletal muscle fibers, where it occurs at discrete sites along the T-tubules (Krolenko and Lucy, 2001); osmotically driven reversible vacuolation in such fibers may function in volume regulation and may facilitate recovery of fatigued muscle fibers. Here, we seek to clarify on experimental and theoretical grounds, what conditions enable rapidly shrinking neurons to form VLDs at discrete sites on their substratum-adherent surface.

Neuronal VLDs (see review in Morris and Homann, 2001) develop exclusively at adherent surfaces. Although cell-mediated events can subsequently pinch off and internalize

Submitted September 25, 2002, and accepted for publication March 24, 2003.

Address reprint requests to C. E. Morris, Neuroscience, Ottawa Health Research Institute, Ottawa Hospital, 725 Parkdale Ave., Ottawa, Ontario, Canada K1Y 4E9. Tel.: 613-798-5555 ext. 18608; Fax: 613-761-5330; E-mail: cmorris@ohri.ca.

0006-3495/03/07/223/13 $2.00

(retrieve) VLD bilayer, we focus here exclusively on the invagination process. In a shrinking neuron, flaccid membrane at nonadherent surfaces would constitute ''excess surface area.'' Net flow from more to less flaccid regions evidently furnishes bilayer for the enlarging VLDs (Mills and Morris, 1998). In large snail neurons, initially tubular invaginations (diameter <1 μm when first visible) can dilate to yield a collection of ballooned-out structures ~ 5 μm across and penetrating a comparable distance into the cytoplasm (Reuzeau et al., 1995). For gradual shrinkage, this occurs in minutes, but abrupt shrinking transitions yield VLDs in a matter of seconds (Dai et al., 1998). Vacuolar appearance notwithstanding, a VLD is an invagination since its lumen is contiguous with bath solution and its bilayer is contiguous with plasma membrane. The number of VLDs per neuron shows an upper limit and when shrink/swell cycles are repeated at 2–3 min intervals, VLDs repeatedly form/reverse at their previous initiation sites (Reuzeau et al., 1995). Evidently, adhesions adjacent to VLD initiation sites are robust enough to survive repeated osmomechanical perturbations. When a VLD-bearing cell is made to re-swell, its VLDs reverse (one might say ''devaginate''), expelling their contents to the bath and presumably the resultant outflow of bilayer relieves tension at the pressurized nonadherent surface (Mills and Morris, 1998).

The inflated look of VLDs suggests that hydrostatic pressure contributes to their formation, but if VLDs are initiated by shrinkage forces pulling inward at patches of membrane skeleton (see Herring et al., 2000) inflation may play a secondary role. Our experimental aim here is to clarify whether hydrostatic pressure dominates early on, making an initial ''pull'' unnecessary. Subsequently, we construct a theoretical framework for hydrostatically-driven invagination. Uncertainty about whether VLDs are pulled or pushed inward arose because 1), maintenance of the dilated state is unrelated to pressure, in that hydrostatic pressure in VLDs would be transient at best, yet VLDs persist indefinitely when formed in the presence of drugs that block energy-driven recovery processes (Reuzeau et al., 1995); and 2), bath dye has ready access (except at actual adhesive contacts) to the narrow gap between neuron and substratum, suggesting that bath osmolytes and water equilibrate quickly—perhaps too quickly to allow for local hydrostatic pressure. Just after VLD formation (1–2 min), bath and VLD lumen dye intensity is equal, and upon bath-dye washout, VLDs clear rapidly.

Accordingly, it was not self-evident that substratum-cell gaps develop transient hydrostatic pressures large enough to inflate VLDs. Although motor (actomyosin) forces do not drive VLD formation (unlike subsequent VLD recovery), the membrane skeleton of nascent VLDs might locally couple shrinking forces to bilayer invagination (Herring et al., 2000; Morris, 2001b). If so, initiation of VLDs might resemble macropinocytosis but with osmomechanical forces, not actomyosin, doing the ''pulling-in'' work (Xu et al., 2001; see also Fig. 1 in Skinner et al. (2001) for massively dilated invaginations in Purkinje cell somata of an ataxic mouse model).

Here, we monitor VLD formation at higher time resolution than previously. Our observations suggest that mismatched re-equilibration rates for water and osmolytes in the cell-substratum gap could transiently yield hydrostatic forces that drive invagination. To formally explore this possibility, we construct a compartmental model of a substratum-adherent cell, and focus on how the extracellular space parameters affect fluxes of water and of bilayer after a shrinking perturbation.

METHODS AND MATERIALS

Monitoring VLD formation by confocal microscopy

FAST DiA oil (4-(4-(dilinoleylamino)styryl)-*n*-methylpyridinium iodide), (D-3897) and Oregon green 488 dextran: 10,000 MW (D-7170) were both purchased from Molecular Probes (Eugene, OR). A stock solution of Fast DiA dissolved in DMSO (5 mM) was stored at -20°C. Immediately before use, Fast DiA staining solution (20 μM/ml) was made by gradually adding 4 μl DiA stock solution to 1 ml normal saline (NS) while sonicating for 2 min. Oregon green 488 dextran was dissolved in NS at 5 mg/ml. This stock solution was stored at -20°C. For microscopy experiments, Oregon green 488 dextran final solution (100 μg/ml) was freshly made by diluting stock solution into NS (for the bath) or into the ''perturbation solutions'' (for micropipettes). Micropipettes tips were broken to ~ 5 μm and filled with dye solution at various osmolarities (perturbation solutions were altered with either distilled water or with sucrose to the osmolarity indicated, but always had dye at 100 μg/ml).

Lymnaea stagnalis neurons were isolated and cultured on uncoated glass as in Herring et al. (1999). At 1–4 d after plating on coverglass ($22 \times 22 \times 0.15$ mm), the neurons were put into a RC-21 bath imaging and recording chamber (Warner Instruments, Hamden, CT). Neurons were first stained by Fast DiA for 20 min at room temperature then washed twice with NS. Oregon green 488 dextran was added to the chamber. Osmotic perturbation of a selected neuron was achieved by lowering a micropipette (filled with Oregon green 488 dextran and the chosen osmolarity) near a particular neuron, and spritzing for ~ 30 s then terminating the spritzing and withdrawing the pipette from the bath. Gentle sustained spritzing of solutions was achieved by supplying a DC voltage to the external input of a General Valve Picospritzer (Warner Instruments) and regulating the supply of compressed nitrogen to the spritzer. Imaging was done on a BioRad MRC 1024 laser scanning confocal microscope (Hemel, Hemstead, Hertsfordshire, UK). For Fast DiA, excitation and emission filters with peaks near 488 and 600 nm (long pass), respectively, were used, and for Oregon green, excitation and emission filters with peaks near 488 nm and 522 nm (bandwidth 35 nm), respectively, were used.

RESULTS

Confocal microscopy

Previously, when we elicited VLDs via whole-bath solution exchanges, unavoidable defocusing/refocusing gave observation deadtimes of 1–2 min. Here, where we elicited VLDs by micropipette spritzing of anisosmotic solutions (at fixed dye concentration), we could monitor VLD formation

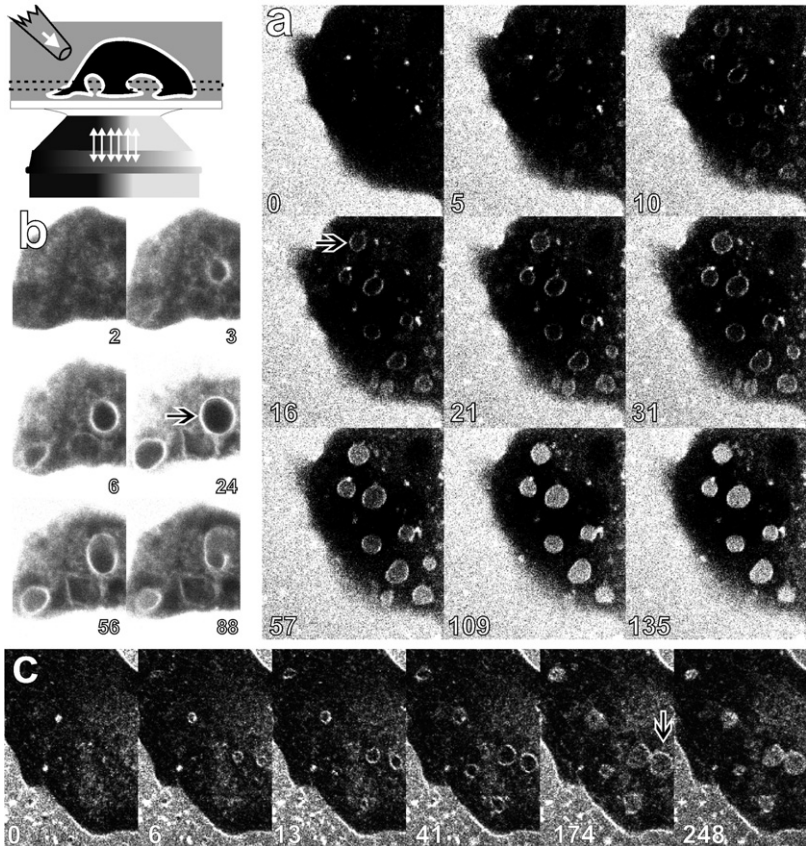

FIGURE 1 Demonstration that water exit across the nascent VLD membrane drives VLD formation. The cartoon in the upper left shows how membrane and bath fluorescence was monitored in a confocal microscope (the *dashed-in* area marginally above the substratum depicts a confocal ''slice''). *Lymnaea* (pond snail) neurons cultured on glass were placed in solution at the same aqueous dye concentration as in the spritzing pipette solution, and the membrane was stained with a lipid dye. The two dyes used (see Methods) had partially overlapping emission spectra and so were both visible in the channel shown here. The pipette was withdrawn from bath after briefly spritzing an imaged cell with an anisosmotic solution. The bath volume was large enough that its osmolarity (normal) was essentially fixed beyond the immediate vicinity of a spritzed neuron. (*a*) Neuron was made to swell (spritzed with 50% snail medium) then was monitored during re-shrinkage in normal snail medium (0–135 s) The arrow points to one of several VLDs that can be seen to have formed with little or no bath dye in their lumens and then subsequently equilibrating with the bath dye. (*b*) Neuron was spritzed with 150% (normal + glucose) snail medium until 26 s, so this series includes both shrinking (2–24 s) and re-swelling (56 s, 88 s). The arrow points to a VLD that formed and began to reverse (see text) without ever equilibrating with the bath dye. (*c*) Neuron was made to swell (spritzed with distilled water) then was monitored as it shrank in normal snail medium (0–248 s). The arrow has the same significance as in *a*.

continuously by confocal microscopy of bath and membrane dye. Experiments using this approach are shown in Fig. 1, which includes images selected from time series for three neurons. Two of the series (Fig. 1, *a* and *c*) are for neurons made to re-shrink in normal medium after swelling (by spritzing with 50% medium, see Fig. 1 *a*; or distilled water, see Fig. 1 *c*) and one (Fig. 1 *b*) is for a neuron made to shrink by spritzing with hyperosmotic medium (until 26 s, when the medium was isoosmotic again, causing the cell to re-swell toward its normal size). Because plasma membrane was pre-stained with a lipophilic dye, the fluorescence images show VLDs forming before having acquired detectable levels of bath dye. In Fig. 1, *a* and *c*, initially dye-free lumens eventually showed bath dye, which became progressively more intense until bath and VLD lumen intensities were indistinguishable. In Fig. 1 *b*, re-swelling was instituted (at 26 s) before any bath dye was evident in the large VLD's lumen. Although not illustrated, the membrane dye was simultaneously imaged in a channel that excluded bath-dye signal; comparisons confirm that VLD lumen intensity increases were not due to membrane dye. Our purpose in showing VLDs forming in neurons shrinking after swelling in 50% and 0% NS, plus a neuron shrinking in hyperosmotic (150%) medium (no prior swelling), is to emphasize that although cell shrinkage is critical, the specifics of the shrinkage protocol are not.

A simple explanation for the images of Fig. 1 is that, as depicted in the cartoon (*upper left*), plasma membrane from the substratum is pushed up into and then through the confocal plane (where before shrinkage, there was non-fluorescent cytoplasm). Adjacent to the nonadherent surface, the bath volume is effectively ''infinite'' whereas the gap volume is a thin disk. Accordingly, as shrinkage (net water exit) commences, both surface area and osmotic driving force are smaller at the gap than at the nonadherent surface. Nevertheless, as the experiments vividly demonstrate, local water movement into the gap continues at a substantial rate, and evidently generates enough hydrostatic pressure to invaginate membrane and displace (or replace) a volume of cytoplasm. When VLDs first become evident in the confocal plane, any aqueous-dye (10,000 MW) present in most of the VLDs illustrated is too dilute to register. Because lower molecular weight bath osmolytes (principally sodium and chloride ions) will re-equilibrate more rapidly than the dextran-dye conjugates, ''dye-free'' signifies ''osmolyte-depleted,'' not osmolyte-free. Osmotic potential (unlike electrical potential) is linear with concentration, so net water flux into the VLD lumen will not precipitously collapse an osmotic driving force. If the substratum membrane acts like a perfect osmometer, a mere 1 mOsm will yield 2.4 kPa (=18 mm Hg), so if the gap impedes water flow, small osmotic gradients may yield hydrostatic pressure transients large

enough to push VLD membrane inward. We note that showing frankly dye-free VLD lumens, as in Fig. 1, is sufficient to support the hypothesis that hydrostatic pressure generates VLDs. Indeed, continuous monitoring of nascent VLDs showed that the lumens of nascent VLD were often initially dye-depleted as opposed to being initially dye-free. However, we think it is important to have captured examples of the starkest, lumen-to-bath differences, namely, the transiently dye-free cases. Quantitative lumen-to-bath differences (lumen dye-intensity measurably lower than bath dye intensity) leave some room for concerns about measured intensity differences from small versus large volumes (e.g., edge effects). Qualitative differences (the transiently dye-free cases) do not.

There are a variety of issues to consider regarding the forces acting on VLD membrane. For argument's sake, let us assume VLD membrane approximates a perfect osmometer. As the cell shrinks, its lost water will not measurably affect bath-dye and osmolyte concentrations except in the gap solution. If the osmolarity gradient across the substratum membrane (cell-to-gap) became, say, 5 mOsm, then at the mouth of a 1 μm hemispheric VLD, the maximum hydrostatic pressure would be 12 kPa. By Laplace's law, this would yield 12 mN/m tension in the membrane or 24 mN/m if the VLD was tubular, not hemispheric. Given the ~10–12 mN/m lytic limit of most biological membranes (including snail neurons; see Dai et al., 1998), 12–24 mN/m would be dangerous. However, VLDs seldom if ever rupture, so something seems to be amiss. If it is not excessive to assume transient 5 mOsm at a VLD mouth during >100 mOsm bath changes, then maybe VLD membrane is not a perfect osmometer during VLD formation. Or perhaps the radius of curvature inferred from light microscopy is too large given that VLDs have a spectrin skeleton (Herring et al 2000; Morris, 2001b) which should ''corrugate'' the bilayer during VLD dilation, lowering the operative tension. To hone our common sense about the range of effects expected from local osmosis where neurons contact a substratum and to serve as a guide to further experiments, we developed a model for VLD formation in isolated adherent cells.

The model

Consider a cell adhering to an inert substratum (see Fig. 2). Let the osmolarity of the cell cytoplasm (expressed in concentration units) be c_c and that in the bath, c_b. At the substratum-adherent part of the cell, the plasma membrane attaches inhomogeneously, creating a cell-substratum gap that is a labyrinth of bath solution whose osmolarity we designate c_v. Solutions flow in the gap and solutes diffuse. At equilibrium, concentrations c_b, c_c, and c_v are equal at an initial value we designate c_0.

At time $t = 0$, c_b is increased. The cell begins to shrink, expelling water to the bath so cell and gap solute concentrations become functions of time: $c_c(t)$ and $c_v(t)$. Bath

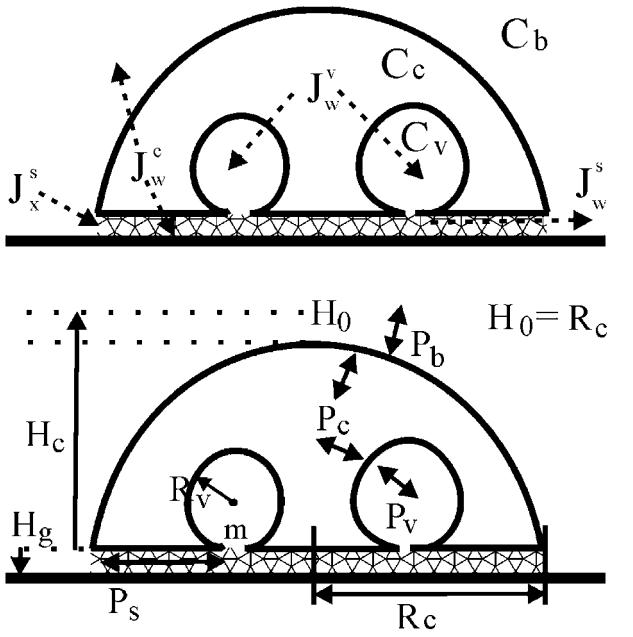

FIGURE 2 Parameters in the model. The VLD-bearing model ''cell'' is depicted twice, first with the concentration and flux parameters, and next with dimensions and pressures. The special porosity and diffusivity characteristics of the adhesion zone are implied by the mesh pattern. The membrane is modeled as a lipid bilayer. Parameters are defined in the text, and some are amplified in the Appendices.

solutes diffusing along the gap change its concentration. After a shrinking perturbation, if the gap's osmolyte concentration increases faster than the cell's, the osmotic imbalance causes net efflux of water across the substratum membrane and into the gap. At points where the membrane is not adherent to the substratum, membrane would tend to bulge inward, thus becoming VLD initiation sites. The fate of these sites is determined by the interplay of fluxes in the system (Fig. 2).

Let the pressure and volume of the cell be p_c and V_c, correspondingly; the same parameters in the VLD are p_v and V_v, and its area is A_v. Due to osmotic imbalance, there is a flux of water from the cell to the VLD:

$$J^v_w = A_v L^v_w [p_c - p_v + RT(c_v - c_c)], \quad (1)$$

where L^v_w is the water permeability coefficient of the invaginating (VLD) membrane (see, for example, Benedek and Villars, 2000). Here we establish the positive sense of flow as cell-to-VLD; the same convention will be used for bath-to-VLD fluxes. Water can also enter VLDs from the bath via the gap along the substratum; this flux can be presented as

$$J^s_w = L^s_w (p_b - p_v). \quad (2)$$

Similarly, the diffusional flux of osmolytes, x, from bath to VLDs along the substratum gap is

$$J^s_x = L^s_x (c_b - c_v), \quad (3)$$

where L_x^s, the ''diffusivity'' coefficient, is the product of the diffusion coefficient D_x and the gap width, with dimensions $\mu m^3\ s^{-1}$. More detailed analysis of this parameter will be given later.

Total flux of water from the shrinking cell is

$$J_w^c = A_c^{free} L_w^c [p_c - p_b + RT(c_b - c_c)] + NJ_w^v, \quad (4)$$

where A_c^{free} is the area of the free surface of the cell, N is the number of VLDs, and L_w^c is the water permeability coefficient of the free cellular membrane. It is assumed to be equal to that of the vacuolar membrane, $L_w^c = L_w^v$.

Due to flaccid character of the nonadherent cell membrane, pressure in the cell p_c can be considered equal to the pressure in the bath:

$$p_c = p_b, \quad (5)$$

while pressure in VLDs is determined by their radius R_v and membrane tension γ:

$$\Delta p = p_v - p_c = \frac{2\gamma}{R_v}, \quad (6)$$

Balance equations

Now we can write the balance equations for the solute concentration and the volume of the VLD:

$$\frac{dc_v}{dt} = \frac{J_x^s - c_v(J_w^v + J_w^s)}{V_v}, \quad (7)$$

$$\frac{dV_v}{dt} = J_w^v + J_w^s. \quad (8)$$

Similar equations for the cell are

$$\frac{dc_c}{dt} = \frac{c_c J_w^c}{V_c}, \quad (9)$$

$$\frac{dV_c}{dt} = -J_w^c. \quad (10)$$

Besides these differential equations for volume and concentration, we assume that during VLD formation the total surface area of the cell remains constant. While membrane capacitance falls continuously for tens of minutes as shrinking neurons undergo the actin-dependent processes of VLD ''recovery'' (Reuzeau et al., 1995; Dai et al., 1998), these events occur, by definition, post-VLD formation. Since VLD membrane is demonstrably invaginated plasma membrane (Mills and Morris, 1998), there are no grounds for postulating bilayer area changes during the few seconds required for VLD formation. Hence, during formation:

$$A_{free} + A_{adherent} + A_{VLD} = A_{tot}. \quad (11)$$

The initial conditions for these equations are

$$c_c(0) = c_v(0) = c_0, \quad (12)$$

$$V_c(0) = V_0, \quad (13)$$

$$V_v(0) = \varepsilon_v. \quad (14)$$

The last equation implies that a small volume underneath the membrane should be included as VLD. This small component is important only at the initial stage of VLD development and can be safely neglected later.

We obtained a set of four differential Eqs. 7–10 for concentration and volume of VLDs and the cell. Our interest is in the VLD characteristics defined by Eqs. 6–8, but these include as a parameter the concentration c_c of cellular osmolytes. For cell shrinkage perturbations, this is actually all we need from Eqs. 9–10. Swelling perturbations, which reverse VLDs, are not explored here, but would be dealt with by modifying Eq. 5.

Cell shrinkage

We visualize the cell on the substratum as a spherical segment with a radius at the adherent surface, R_c, and height H_c (Fig. 2). The initial height is $H_0 = R_c$. The upper surface, constituting more than one-half of the surface area, would support most of osmotic flux of water. The radius R_c of the adherent cell's base is fixed. The volume of the cell and its free area can be presented as follows:

$$V_c = \frac{1}{6}\pi H_c(3R_c^2 + H_c^2), \quad (15)$$

$$A_{free} = \pi(R_c^2 + H_c^2). \quad (16)$$

The initial volume and free area of the cell are

$$V_c(0) = \frac{2}{3}\pi R_c^3 \quad \text{and} \quad A_{free}(0) = 2\pi R_c^2. \quad (17)$$

In the case of flaccid cells (no hydrostatic pressure difference from cell-to-bath), Eqs. 9–10 reduce to

$$\frac{dc_c}{dt} = \frac{6L_w^c RTc_c(c_b - c_c)(R_c^2 + H_c^2)}{H_c(3R_c^2 + H_c^2)}, \quad (18)$$

$$\frac{dH_c}{dt} = -2L_w^c RTc_0\left[\frac{c_b}{c_0} - \frac{4R_c^3}{H_c(3R_c^2 + H_c^2)}\right]. \quad (19)$$

This system includes two characteristic parameters: one is the cell radius, R_c, and the second is a parameter of velocity

$$u = L_w^c RTc_0. \quad (20)$$

Their ratio gives the characteristic time of the shrinking process:

$$\tau_c = \frac{R_c}{L_w^c RTc_0}. \quad (21)$$

Now let us estimate this τ_c (Eq. 21). We assume an internal osmolarity of the cell equal to the osmolarity of a typical mammalian neuron, $c_0 = c_{MN} = 0.29$ Osm, and the

radius of the cell $R_c = 25\ \mu$m. Using the other values from Appendix B, ''Constants and Parameters,'' one can find characteristic velocity $u_{MN} = L_w^c RT c_{MN} = 7.34 \times 10^{-7}$ m $s^{-1} = 0.734\ \mu$m s^{-1}, and the characteristic time of shrinking:

$$\tau_c = \frac{R_c}{L_w^c c_{MN} RT} = \frac{25 \times 10^{-6}}{10^{-7}\, 7.34} = 34\ \text{s}. \tag{22}$$

Using these numbers, one can solve these equations numerically. Fig. 3 shows how the height of the cell and concentration of its osmolytes change after bath concentration doubles. Notice that the cell's half-maximum concentration change occurs at the moment $t_{1/2} = 0.26$, $\tau_c = 8.8$ s.

How much area is retrieved from the top of the cell during shrinkage? It is equal to

$$A_{\text{retrieved}}(t) = A_{\text{free},0} - A_{\text{free}} = \pi(R_c^2 - H_c^2), \tag{23}$$

where $A_{\text{free},0}$ is the initial free area. This function is presented in Fig. 4.

It is convenient to present the equations of this section in dimensionless form by normalizing time by τ_c, concentrations by c_0, and lengths by R_c:

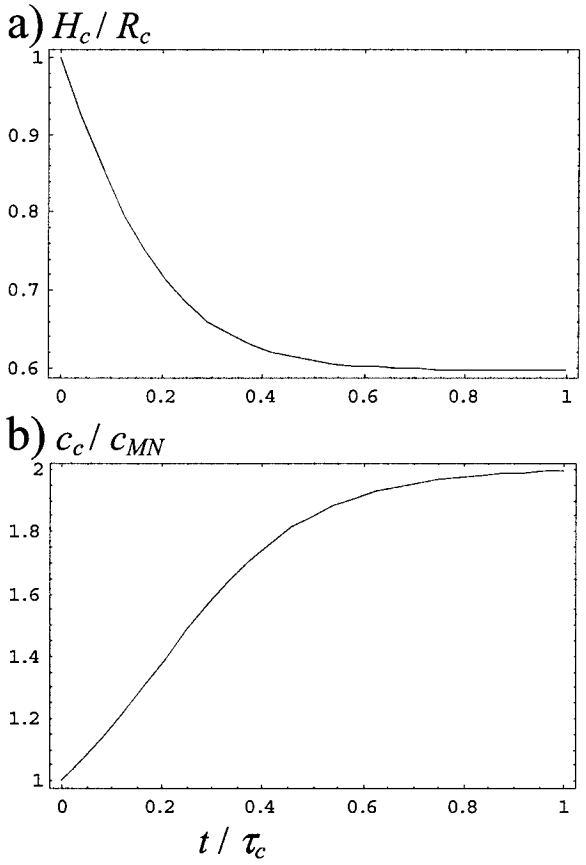

FIGURE 3 Timecourses for the height of the cell (*a*) and its osmolyte concentration (*b*), $c_0 = c_{MN}$ and $c_b/c_0 = 2$.

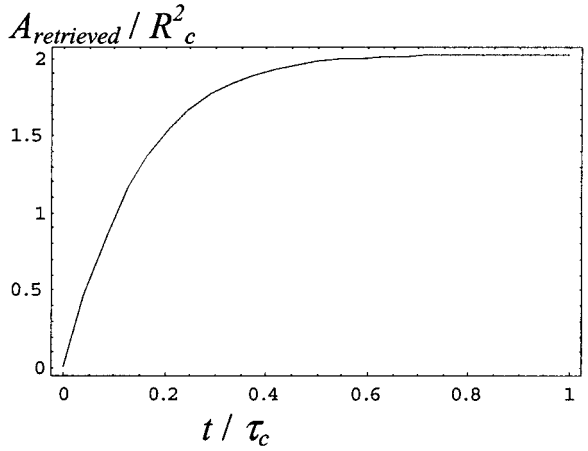

FIGURE 4 Timecourse for the growth of total VLD surface area.

$$\theta = \frac{t}{\tau_c},\ \ \zeta_c = \frac{c_c}{c_0},\ \ \zeta_b = \frac{c_b}{c_0},\ \ \zeta_v = \frac{c_v}{c_0},\ \ h = \frac{H_c}{R_c},$$
$$a_{\text{retrieved}} = \frac{A_{\text{retrieved}}}{R_c^2}. \tag{24}$$

Then the main equations will assume a very concise form (as noted by an unknown reviewer, Eqs. 25 and 26 can be solved analytically to find a rather interesting time-independent property of this relationship, ζ_c as a function of h_c; however, here we are mainly interested in the time variation of concentration, ζ_c (θ), as calculated in the following sections):

$$\frac{d\zeta_c}{d\theta} = \frac{6\zeta_c(\zeta_b - \zeta_c)(1 + h_c^2)}{h_c(3 + h_c^2)}, \tag{25}$$

$$\frac{dh_c}{d\theta} = -2\left[\zeta_b - \frac{4}{h_c(3 + h_c^2)}\right], \tag{26}$$

$$a_{\text{retrieved}} = \pi(1 - h_c^2). \tag{27}$$

VLD growth

VLD formation and growth is determined by fluxes of solute J_x^s along the substratum and by osmotic flux of water J_w^v across VLD membrane. If we neglect the role of hydrostatic pressure for concentration variation, then the equations for VLD can be presented as follows:

$$\frac{dc_v}{dt} = \frac{3L_x^s(c_b - c_v)}{4\pi R_v^3} - \frac{3L_w^v RT c_v(c_v - c_c)}{R_v}, \tag{28}$$

$$\frac{dR_v}{dt} = L_w^v RT(c_v - c_c). \tag{29}$$

Here, we assumed that VLDs are spherical and switched from the VLD volume to its average radius R_v.

Switching here to the dimensionless form we introduce

$$\rho_v = \frac{R_v}{R_c}, \quad \lambda_x^s = \frac{L_x^s}{L_w^v R_c^2 RTc_0}. \tag{30}$$

Thus, parameter λ_x^s is the ratio of diffusional permeability of osmolytes in the gap (L_x^s) to the water permeability of VLD membrane (denominator) with an appropriate coefficient to make the ratio dimensionless. If one divides Eq. (28) by $L_w^v RTc_0^2/R_c$ and Eq. (29) by $L_w^v RTc_0$, then this set of equations reduces to:

$$\frac{d\zeta_v}{d\theta} = \frac{3\lambda_x^s(\zeta_b - \zeta_v)}{4\pi\rho_v^3} - \frac{3\zeta_v(\zeta_v - \zeta_c)}{\rho_v}, \tag{31}$$

$$\frac{d\rho_v}{d\theta} = \zeta_v - \zeta_c. \tag{32}$$

Let us analyze these equations. Concentration in the VLD is described by Eq. 28 or 31 by the two terms on the right-hand side of this equation. The first term presents the flux of osmolytes along the substratum under the gradient of concentration. Dividing this flux by the VLD volume converts it to a concentration; hence, we find R^3 in the denominator of this term. The second term, which is negative, describes the dilution of the VLD content due to osmotic flow of water from the cell. The presence of R^3 in the first term makes it dominate just after a perturbation when the VLD is very small. Therefore c_v will grow very quickly to c_b. The further development will depend on the relationship between the two terms in Eq. 31. There are two limiting cases.

Limiting case 1: fast lateral osmolyte diffusion in the gap

If $\lambda_x^s \gg 4\pi\rho_v^2$, the first term always remains predominant. Then the concentration in the VLD remains equal to ζ_b and does not depend on time.

Limiting case 2: fast water permeation across VLD membrane

If condition $\lambda_x^s \gg 4\pi\rho_v^2$ is not fulfilled, then water flux through the VLD membrane can become the determining factor. The behavior of the cell becomes more complicated. We follow the time course of three parameters: c_c, c_v, and R_v. The result depends on the specific value of the coefficient for diffusional transport of the osmolyte, L_x^s. Figs. 5–8 present parameters of the system for four selected values of λ_x^s. In all cases c_c steadily increases from c_0 to c_b. The VLD concentration, c_v, at the start of a shrinking perturbation jumps from c_0 to c_b and then starts to decline. Although the speed of this initial jump depends on L_x^s, it is too fast to be resolved at this scale. Over time, c_c passes through a minimum and then goes to the new c_b. The amplitude of this transient depends on L_x^s.

The average VLD radius increases monotonically with time and eventually reaches a maximum. If λ_c^s if very large, this radius is ~5 μm, but for smaller λ_x^s, the radius drops (e.g., $\lambda_x^s = 0.01$, R = 1.5 μm).

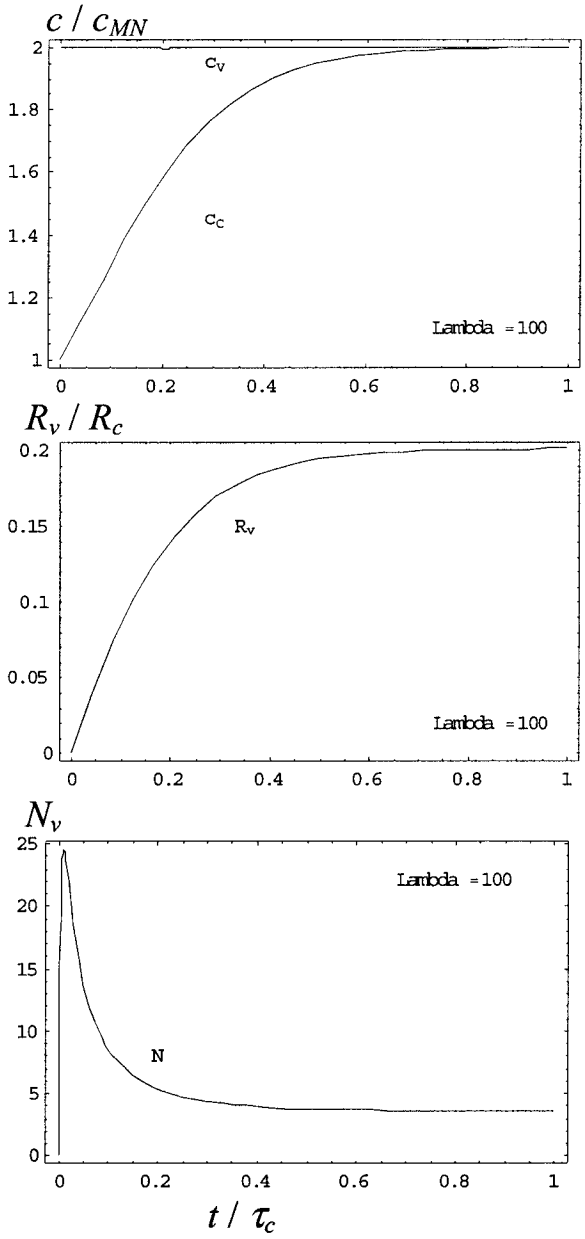

FIGURE 5 For λ_x^s (lambda) = 100, timecourses for various VLD parameters. As defined in Eq. 30, $\lambda_x^s = L_x^s/L_w^v R_c^2 RTc_0$. Note that although L_x^s has dimensions of $\mu m^3\ s^{-1}$, λ_x^s is dimensionless.

Number of VLDs

Having calculated the area retrieved, $A_{retrieved}$, from the upper part of the cell at any moment of time and knowing how R_v, the average VLD radius changes with time, we can find the maximum number of VLDs a cell can form if there is no other source of membrane:

$$N_v = A_{retrieved}/4\pi R_v^2. \tag{33}$$

This function is also presented in Figs. 5–8. In these calculations we arbitrarily did not consider VLDs < 0.5 μm

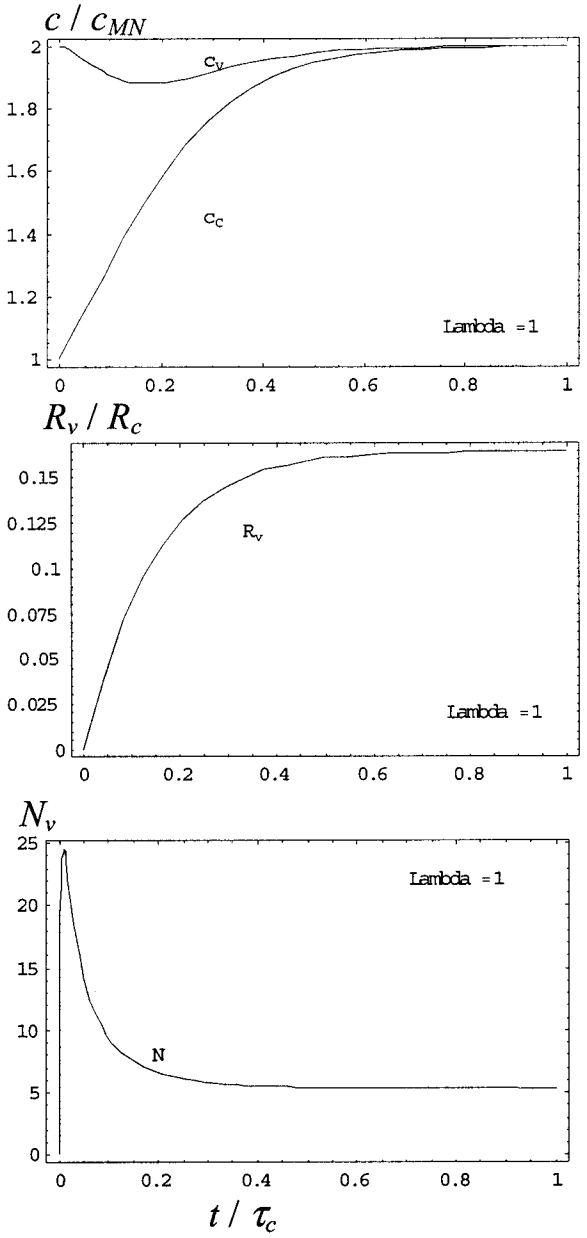

FIGURE 6 For $\lambda_x^s = 1$, timecourses for various VLD parameters.

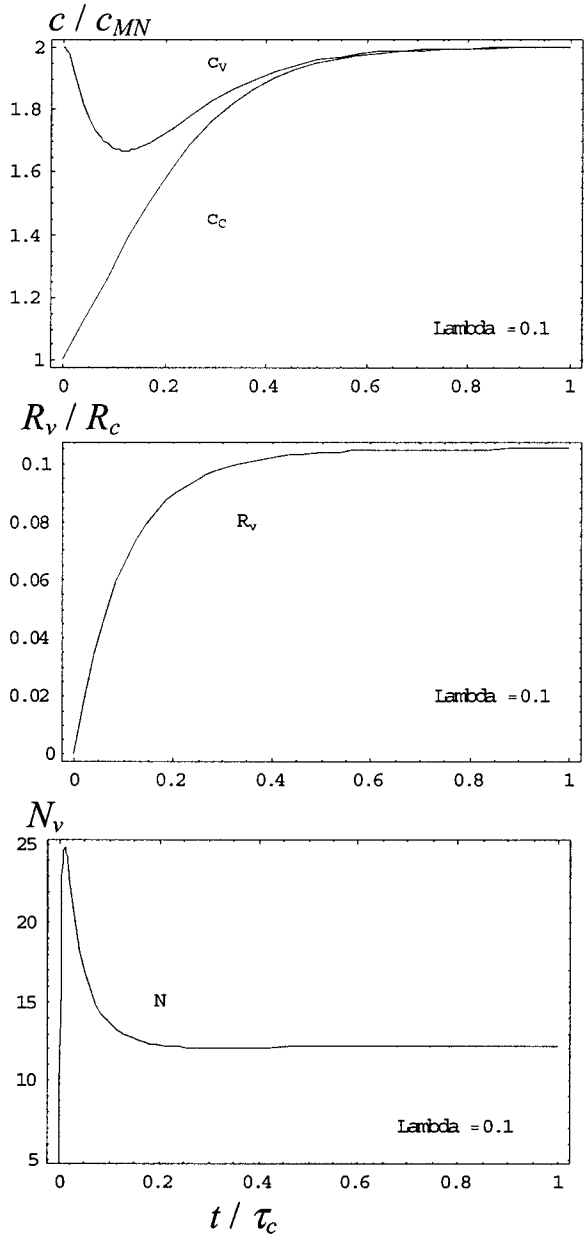

FIGURE 7 For $\lambda_x^s = 0.1$, timecourses for various VLD parameters.

in diameter. One can see that the number of VLDs starts at ~25, then decreases to 4, or 5, or 12, depending on λ_x^s. However, if λ_x^s is <0.02, the number of VLDs increases monotonically.

In Figs. 5–7, VLDs numbers first increase then decrease, so in effect, VLDs interact with each other, with bigger ones ''devouring'' small ones. This arises from pressure/tension differences among VLDs. As VLDs are initiated, some, because of their location along the diffusional gradients in the gap, will feel more hydrostatic pressure than others. The higher pressure VLDs will enlarge faster and their resultant larger radii will dictate higher membrane tensions (for given pressures) than what is felt in neighboring smaller VLDs. Accordingly, larger ones will tend to acquire bilayer from their surround, a surround that includes the smaller (rapidly disappearing) VLDs. Thus, bilayer scavenging by the dominant VLDs operates in a positive-feedback mode for a short time before osmotic equilibrium.

VLDs might initiate surface area regulation in shrinking cells, but even as invaginations (before any endocytic activity) their displacement of a volume of cytoplasm could be useful. From a tissue point of view, their pseudo-intracellular-volume character may have interesting consequences. In CNS tissue, where nests of cells are variously swelling and shrinking, VLDs could facilitate the maintenance of tissue volume within a narrow range. In Fig. 9 we plot the total

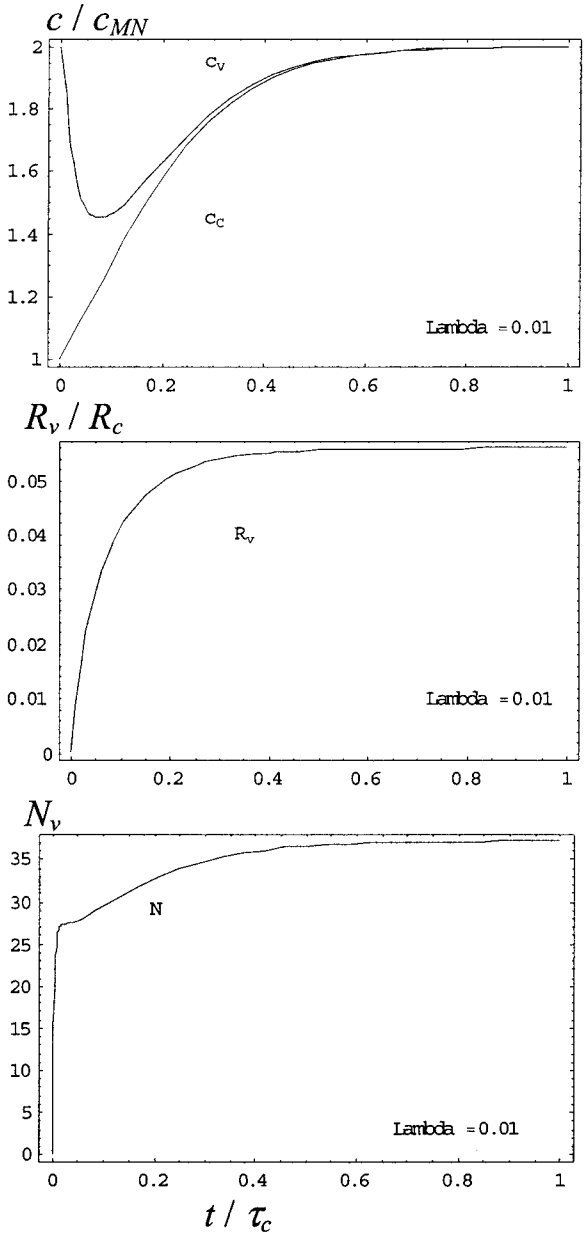

FIGURE 8 For $\lambda_x^s = 0.01$, timecourses for various VLD parameters.

displaced volume for low, intermediate values of lambda ($\lambda_x^s = 0.01$, 1, 100), the ratio of diffusional permeability of osmolytes in the gap to the water permeability across VLD membrane. The equilibrium volumes displaced by VLDs in these three cases are ~1.2% to ~6% of the initial cell volume; because cell volume falls to one-half, this means 2.5–12% of the final volume. If a larger fraction of cell surface was adherent at the outset (as in the CNS), then even larger displaced volumes could pertain. Note also that because of surface area/V considerations raised earlier, parameter sets that favor fewer larger VLDs should produce greater overall displacements.

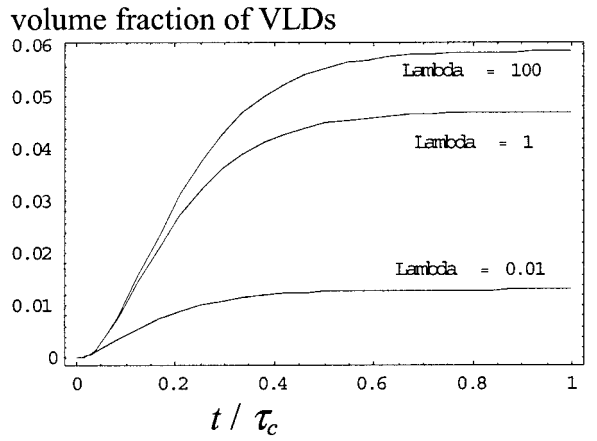

FIGURE 9 For $\lambda_x^s = 100$, 1, and 0.01, timecourses for VLD growth (as a fraction of total cell volume).

DISCUSSION

Real and model cells

We examined experimentally and theoretically the consequences of rapid shrinkage in a cell adhering to a substratum. Our focus was the formation of membranous invaginations (VLDs) at the adherent surface.

Uninterrupted monitoring of bath-dye intensity in nascent VLDs showed that water exit at the adherent surface could be fast enough to generate initially bath-dye-free VLDs. The inescapable implication: hydrostatic pressure resulting from this local osmosis could initiate and inflate VLDs. Before this demonstration (Mills and Morris, 1998) an alternate scenario (see Morris and Homann, 2001) had to be taken seriously in which VLDs are initiated like macropinosomes, with an initial inward pull establishing VLD sites (see Lee and Knecht, 2002, for the pulling-in event of macropinocytosis). Pulling-in was entertained because newly-formed VLDs were always seen to have the same dye intensity as the bulk bath solution (like the 135 s image of Fig. 1 *a*). However, the better time resolution achieved here let us capture VLDs that were not only transiently dye-depleted but in some cases even transiently dye-free. In contemplating the likely magnitude of hydrostatic and hydrodynamic effects in submicroscopic biospaces, ''common sense'' interpolations from macroscopic systems are inadequate to the task. A case in point is the still-active decades-old controversy among students of epithelial fluid secretion over the role (or not) of intercellular space local osmosis (Spring, 1999; Loo et al., 2002). It was therefore not merely a trivial exercise to directly demonstrate, as we did here, a transient increase in water concentration at a locale postulated to transiently sustain a hydrostatic pressure.

The cell depicted in the model was essentially a large adherent liposome with part of its surface making a labyrinthine area of adhesive contact to a flat substratum. Several

issues we encountered in setting parameters and constants are worth highlighting. For simplicity we made the resting cell flaccid (no resting membrane load) and hence ''membrane tension'' has meaning only at the VLDs, and only during osmotic equilibration. The nonzero tension measured in neurons at rest (Dai et al., 1998) arises principally from bilayer-cytoplasm interactions, and should, all else being equal, have little effect on the details of VLD formation, since water efflux rates (not bilayer tension) are probably limiting. The limited knowledge of osmolyte diffusion coefficients in restricted biospaces is an issue, but we note that co-efficients obtained using new fast optical methods are not remarkably different from values for free solution (e.g., Xia et al. 1998). Our approach was to describe diffusion in the cell-substratum gap by lumping porosity and tortuosity as an ''effective diffusion co-efficient.'' Since this diffusivity term is not only unknown but can be expected to vary, we varied it in the guise of gap height changes (see Appendix B).

The model robustly predicts that during cell shrinkage, excess bilayer from the flaccid nonadherent surface will flow toward the substratum and invaginate as multiple VLDs along the adherent surface. Details of this process (rate of change of VLD lumenal concentration; speed of dilation; number and size of VLDs at equilibrium) depend on how the cell-substratum gap parameters (i.e., extracellular space, i.e., ECS, geometry) affects. The importance of ECS geometry is summarized in Fig. 10 *a, i–iii*. Where the ECS presents little effective restriction to diffusion (Fig. 10 *ai*) or where that restriction is extreme (Fig. 10 *aiii*), VLDs do not form because neither situation allows for osmomechanical forces to build up locally. Shrinkage-induced invaginations occur where there is an intermediate degree of restriction to lateral diffusion (Fig. 10 *aii*). Fig. 10 *b* is meant to suggest that inhomogeneous substratum-cell adhesivity and inhomogeneous gap thickness (expected in vivo but not included in the model) would tend to randomize any spatial patterns for VLDs.

The extent and timecourse of VLDs formation in our experiments and our model depends partly on the use of step osmotic perturbations. Osmotic imbalances experienced by healthy CNS neurons will be noninstantaneous and, generally, cell-mediated rather than exogenous. Neurons swell when intense activity generates excess intracellular osmolytes, then they shrink because of cell-mediated volume regulatory processes (e.g., Darquie et al., 2001: Pasantes-Morales et al., 2000; Takagi et al., 2002; Patel et al., 1998). Neurons in transiently hyperstressed CNS nuclei exhibit reversible vacuolation (e.g., Hargreaves et al., 1994; Wu and Casida, 1996). The phenomenon is seen as reflecting near-death pathology, but note that if pathology includes damaged trafficking of surface membrane (e.g., Skinner et al., 2001) it may well include damaged surface area regulation, and hence excessively big, nonrecovering VLDs. According to the model, the critical factor for forming VLDs is an osmolyte concentration at VLD mouths exceeding that in the cell. Intra- and extracellular osmolarity changes could both contribute. In situ, potential ''mouths'' would be patches of lightly-anchored or non-anchored membrane in otherwise strongly adherent surfaces. Unlike our cell culture and mathematical models, neurons in situ adhere not to an inert substratum but to other osmotically and metabolically active cells or to extracellular matrices. Moreover, osmolytes pumped or dumped into restricted extracellular spaces (ECS) from hyperactive neurons might elicit VLD formation in, say, adjacent glia (hippocampal glia readily form VLDs; C. E. Morris and L. R. Mills, unpublished observation).

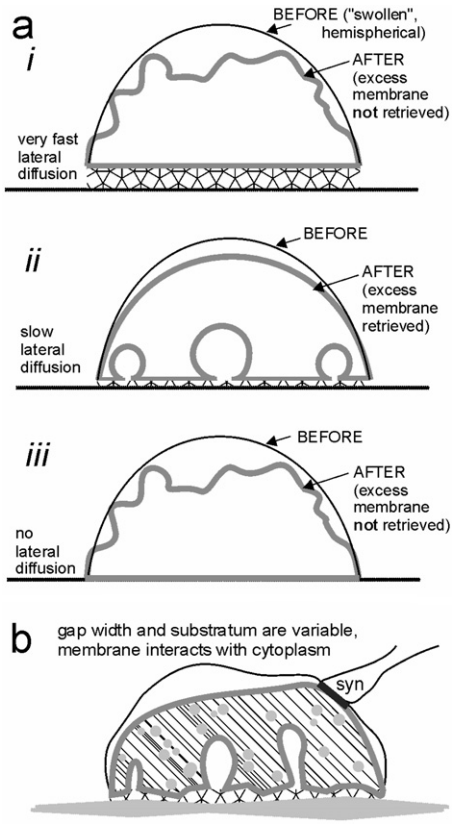

FIGURE 10 Behavior of the model for extreme values of L_x^s, the diffusional permeability of osmolytes in the cell-substratum gap; *a* summarizes the consequence of having (*i*) extremely large, (*ii*) intermediate, or (*iii*) extremely small values of L_x^s. As soon as shrinking begins, membrane in the nonadherent regions of the cell becomes flaccid, but only for intermediate values of L_x^s can this excess be ''retrieved'' in the form of VLDs. The equilibrium size of particular VLDs varies according to the particular rates at which hydrostatic pressure and chemical potentials dissipate. As suggested in *b* for real cells, irregularities in gap width and porosity/diffusivity characteristics along the substratum would be expected to produce irregular distributions of VLD sizes. A synapse (''syn'') is shown to emphasize the strongly adhesive contact at synapse (recall that these structures are stable enough to survive the mechanical rigors of synaptosome preparations), and would be less likely sites for VLD initiation than extrasynaptic membrane.

Local osmosis as a regulatory agent in the CNS

During the osmotic stress associated with intense neural activity, the tortuous gaps of central nervous system ECS have well-established consequences for electrical signaling and volume transmission. We postulate that, additionally, during intense activity, ECS geometry may foster the formation of invaginations. Overall, this could help preserve neuronal connectivity after swelling (Morris, 2001a). Small scale VLDs might contribute to the unexpectedly high ECS tortuosity (seen from tracer dynamics) of shrinking brain slice preparations (Fig. 11) (see Chen and Nicholson, 2000). In their model for shrinkage of central neurons, Chen and Nicholson have water exit causing all cells to move away from each other, with nonuniformity of cell shape giving rise to scattered ECS ''lakes.'' Tracers undergo extended random walks in these lakes and hence, tortuosity diminishes less than expected. Although Chen and Nicholson incorporate no blindly-ending invaginations in their model (see Fig. 11), they do point to theoretical work showing that ''dead-end pores'' (a term that would apply to VLDs) elevate tortuosity. We offer the following observations: 1), Widespread, possibly devastating, disruption of the perineuronal net (Matthews et al., 2002) and the panoply of ''smart glue molecules'' (see Ryan, 2001) that maintain cell-cell contacts in the nervous system would ensue if all central neurons and glia mutually moved away from each other. 2), Tacitly assumed in the Chen and Nicholson model is that instantaneous (on the timescale of the osmotic perturbations) adjustment of surface area occurs when cell volume increases and decreases, with a second order assumption that these surface area adjustments have no consequences for tortuosity. In osmotically dynamic regions of the CNS, we think, surface area adjustments driven by local osmosis may contribute to the preservation of cell-cell interactions. In Fig. 11 (*bottom*), we suggest that there might be interesting consequences if surface area regulation (in the guise of reversible VLD formation) were made explicit in the Chen and Nicholson model (see Fig. 11 legend for details). If invaginations inflated as pseudo-intracellular compartments in shrinking cells, as suggested, a direct dividend would be that exiting water could work to push adherent cells together rather than apart, minimizing stress on information-rich cell-cell adhesions, including, presumably, synaptic contacts. If, moreover, it is osmotically-driven invaginations that increase ECS tortuosity (rather than ''ecs lakes'' created by cells moving away from each other), then the experimentally observed relationship between ECS tortuosity and ECS osmolarity (Krizaj et al., 1996; Tao, 1999) may apply even for the nonpathological cell volume transients of highly-active, communicating neurons. This should, note, diminish zone-to-zone crosstalk via volume transmission, and conversely, impaired surface area regulation would foster unwanted volume transmission. These suggestions take on added interest with the finding that even moderate levels of neural activity can result in a temporary surfeit of surface membrane (Sun et al., 2002).

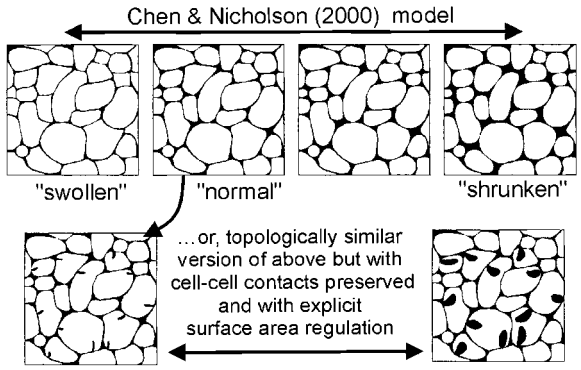

FIGURE 11 VLDs and ECS in the brain. Based on experimental and theoretical studies of brain slice ECS, Chen and Nicholson (2000) postulate that shrinkage creates ECS ''lakes.'' They tested ECS/cytoplasm ratios of 0.13, 0.16, 0.18, and 0.22; the geometry they used is as shown along the top panel. Shrinkage is seen as causing cells to mutually pull away from each other. Although surface area is tacitly depicted as regulated (it rises and falls with swelling and shrinking, respectively), this is deemed not relevant to changing ECS tortuosity. However, what if, 1), cell-cell contacts *are* mostly maintained, and 2), surface area regulation generates dilated invaginations akin to VLDs? Then it would seem appropriate to recast Chen and Nicholson along the lines suggested at bottom. We labeled the ECS/cytoplasm = 0.16 situation as ''normal'' simply for convenience, since we can then use the 0.13 situation as ''swollen.'' A ''shrink'' (using artistic license to add VLDs) brings this same 0.16 diagram to an ~0.22 situation. New ECS diffusion traps (in the guise of VLDs) still appear during swell/shrink perturbations, but surface area regulation is explicit and cell-cell contacts are not ruptured as cells shrink. ''Normal'' (ECS/cytoplasm = 0.16) is provided at bottom, with nascent surface invaginations which allow for reversible swell/shrink perturbations. Alternatively, we could have tacitly assumed mechanically-accessible *endo*membrane stores to allow for swelling (see Morris and Homann, 2001). Such stores are implicit in the Chen and Nicholson model, but they (implicitly) respond instantly and perfectly to swell/shrink perturbations and so are ignored with regards to tortuosity. Cell-cell adhesions are also implicit in Chen and Nicholson, but are depicted as being extremely (perhaps abnormally?) extensible. Putting surface area adjustment along the lines shown here into the Chen and Nicholson model should, we suspect, strengthen its central message—namely, that shrinkage causes increased ECS tortuosity. For intact tissues, however, it remains to be demonstrated if either scenario pertains. If they do, then regions where hyperactive neurons and glia are deploying volume regulatory machinery should transiently exhibit both small VLDs and localized tortuosity increases.

APPENDIX A: DIFFUSION OF THE SOLUTE ALONG SUBSTRATE

Here we estimate parameters of diffusion flux in the space between substrate and the cell. Let this gap have the height H_g. Not all the space of the gap is available for diffusion because of the contact between the cell and substratum, and the path of diffusion might be very tortuous. We account for both porosity and tortuosity with the coefficient η so that effective diffusion coefficient can be presented as $D_{eff} = \eta D$. Let us consider a VLD with the radius of its ''mouth'' R_m in the middle of the cell (Fig. 2). Diffusion of the solute from the bath to this VLD is described by the equation

$$\frac{\partial c_g}{\partial t} = \frac{1}{r}\frac{\partial}{\partial r}\left(rD_{eff}\frac{\partial c_g}{\partial r}\right). \quad (A1)$$

If concentration at the mouth of the VLD is c_v, then the steady-state solution of this equation is

$$c_g = \frac{c_v \ln\frac{R_c}{r} + c_b \ln\frac{r}{R_m}}{\ln\frac{R_c}{R_m}}. \quad (A2)$$

Steady-state total flux coming to the ''mouth'' of the VLD is

$$J_c^s = \frac{2\pi H_g D_{eff}(c_b - c_v)}{\ln(R_c/R_m)}. \quad (A3)$$

Comparing with Eq. 3, one can find

$$L_c^s = \frac{2\pi H_g \eta D}{\ln(R_c/R_m)}. \quad (A4)$$

Now we can estimate the coefficient L_c^s. Using diffusion coefficient $D = 10^3$ $\mu m^2\ s^{-1}$ and arbitrarily assuming that $R_c = 25\ \mu m$, $R_m = 0.5\ \mu m$, $H_g = 0.1$ μm, and $\eta = 0.1$, one can find $L_c^s = 16\,\mu m^3\ s^{-1}$ and $\lambda_x^s = 0.035$. The estimates for R_c and R_m are about right, whereas H_g and η are not known, and would be expected to vary. Therefore L_c^s and λ_x^s can vary for, say, an order of magnitude. These possible departures were incorporated in Figs. 5–8. However, this was calculated for the center of the cell and the gap was assumed to be very narrow (0.1 μm). For the wider gap and more peripheral VLDs, λ can be much higher, in the range of that considered above.

APPENDIX B: CONSTANTS AND PARAMETERS

1 Osm = 1 osmol/Liter^{-1}, which generates osmotic pressure of 2.57×10^6 Pa at temperature 37°C.

Mammalian neuron (MN) osmolarity is $c_{MN} = 0.29$ Osm.

Osmotic pressure of MN is $c_{MN}\,RT = 7.436 \times 10^5$ Pa = 7.34 atm.

L_w for lipid membranes is $\sim 10^{-7}$ m s^{-1} atm^{-1}.

Parameter of velocity is $\mu_{MN} = L_w\,RT\,c_{MN} = 7.34 \times 10^{-7}$ m s^{-1} = 0.734 $\mu m\ s^{-1}$, which is the swelling velocity of a mammalian neuron placed in distilled water.

$R_c = 25\ \mu m$.

$H_0 = R_c = 25\ \mu m$.

$R_{v,max} = 5\ \mu m$.

$\tau_c = 34$ s.

Constant of length is $R_c = 25\ \mu m$.

This work was supported by a grant to C.E.M. from the Heart and Stroke Foundation of Ontario (T4436).

REFERENCES

Aitken, P. G., A. J. Borgdorff, A. J. Juta, D. P. Kiehart, G. G. Somjen, and W. J. Wadman. 1998. Volume changes induced by osmotic stress in freshly isolated rat hippocampal neurons. *Pflugers Arch.* 436:991–998.

Benedek, G. R., and F. M. H. Villars. 2000. Physics with illustrative examples from medicine and biology. *In* Statistical Physics. Springer-Verlag, New York.

Bray, D., N. P. Money, F. M. Harold, and J. R. Bamburg. 1991. Responses of growth cones to changes in osmolality of the surrounding medium. *J. Cell Sci.* 98:507–515.

Chen, K. C., and C. Nicholson. 2000. Changes in brain cell shape create residual extracellular space volume and explain tortuosity behavior during osmotic challenge. *Proc. Natl. Acad. Sci. USA.* 97:8306–8311.

Chklovskii, D. B., T. Schikorski, and C. F. Stevens. 2002. Wiring optimization in cortical circuits. *Neuron.* 34:341–347.

Cooney, J. R., J. L. Hurlburt, D. K. Selig, K. M. Harris, and J. C. Fiala. 2002. Endosomal compartments serve multiple hippocampal dendritic spines from a widespread rather than a local store of recycling membrane. *J. Neurosci.* 22:2215–2224.

Czekay, R. P., E. Kinne-Saffran, and R. K. Kinne. 1994. Membrane traffic and sorbitol release during osmo- and volume regulation in isolated rat renal inner medullary collecting duct cells. *Eur. J. Cell Biol.* 63:20–31.

Dai, J., M. P. Sheetz, X. Wan, and C. E. Morris. 1998. Membrane tension in swelling and shrinking molluscan neurons. *J. Neurosci.* 18:6681–6692.

Darquie, A., J. B. Poline, C. Poupon, H. Saint-Jalmes, and D. Le Bihan. 2001. Transient decrease in water diffusion observed in human occipital cortex during visual stimulation. *Proc. Natl. Acad. Sci. USA.* 98:9391–9395.

Hargreaves, R. J., R. G. Hill, and L. L. Iversen. 1994. Neuroprotective NMDA antagonists: the controversy over their potential for adverse effects on cortical neuronal morphology. *Acta Neurochir. Suppl.* 60: 15–19.

Herring, T. L., P. Juranka, J. McNally, H. Lesiuk, and C. E. Morris. 2000. The spectrin skeleton of newly-invaginated plasma membrane. *J. Muscle Res. Cell Motil.* 21:67–77.

Herring, T. L., C. S. Cohan, E. A. Welnhofer, L. R. Mills, and C. E. Morris. 1999. F-actin at newly invaginated membrane in neurons: implications for surface area regulation. *J. Membr. Biol.* 171:151–169.

Ikegaya, Y., J. A. Kim, M. Baba, T. Iwatsubo, N. Nishiyama, and N. Matsuki. 2001. Rapid and reversible changes in dendrite morphology and synaptic efficacy following NMDA receptor activation: implication for a cellular defense against excitotoxicity. *J. Cell Sci.* 114:4083–4093.

Krizaj, D., M. E. Rice, R. A. Wardle, and C. Nicholson. 1996. Water compartmentalization and extracellular tortuosity after osmotic changes in cerebellum of *Trachemys scripta*. *J. Physiol.* 492:887–896.

Krolenko, S. A., and J. A. Lucy. 2001. Reversible vacuolation of T-tubules in skeletal muscle: mechanisms and implications for cell biology. *Int. Rev. Cytol.* 202:243–298.

Lee, E., and D. A. Knecht. 2002. Visualization of actin dynamics during macropinocytosis and exocytosis. *Traffic.* 3:186–192.

Loo, D. D., E. M. Wright, and T. Zeuthen. 2002. Water pumps. *J. Physiol.* 542:53–60.

Matthews, R. T., G. M. Kelly, C. A. Zerillo, G. Gray, M. Tiemeyer, and S. Hockfield. 2002. Aggrecan glycoforms contribute to the molecular heterogeneity of perineuronal nets. *J. Neurosci.* 22:7536–7547.

Mills, L. R., and C. E. Morris. 1998. Neuronal plasma membrane dynamics evoked by osmomechanical perturbations. *J. Membr. Biol.* 166:223–235.

Morris, C. E. 2001a. Mechanosensitive membrane traffic and an optimal strategy for volume and surface area regulation in CNS neurons. *Am. Zool.* 41:721–727.

Morris, C. E. 2001b. Mechanoprotection of the plasma membrane in neurons and other nonerythroid cells by the spectrin-based membrane skeleton. *Cell. Mol. Biol. Lett.* 6:703–720.

Morris, C. E., and U. Homann. 2001. Cell surface area regulation and membrane tension. *J. Membr. Biol.* 179:79–102.

Nicholson, C., K. C. Chen, S. Hrabetova, and L. Tao. 2000. Diffusion of molecules in brain extracellular space: theory and experiment. *Prog. Brain Res.* 125:129–154.

Patel, A. J., I. Lauritzen, M. Lazdunski, and E. Honore. 1998. Disruption of mitochondrial respiration inhibits volume-regulated anion channels and provokes neuronal cell swelling. *J. Neurosci.* 18:3117–3123.

Pasantes-Morales, H., R. Franco, M. E. Torres-Marquez, K. Hernandez-Fonseca, and A. Ortega. 2000. Amino acid osmolytes in regulatory volume decrease and isovolumetric regulation in brain cells: contribution and mechanisms. *Cell. Physiol. Biochem.* 10:361–370.

Reuzeau, C., L. R. Mills, J. A. Harris, and C. E. Morris. 1995. Discrete and reversible vacuole-like dilations induced by osmomechanical perturbation of neurons. *J. Membr. Biol.* 145:33–47.

Ryan, T. A. 2001. NCAM and vesicle cycling: the importance of good glue in the long run. *Neuron*. 32:759–761.

Skinner, P. J., C. A. Vierra-Green, H. B. Clark, H. Y. Zoghbi, and H. T. Orr. 2001. Altered trafficking of membrane proteins in Purkinje cells of SCA1 transgenic mice. *Am. J. Pathol.* 159:905–913.

Spring, K. R. 1999. Epithelial fluid transport—a century of investigation. *News Physiol. Sci.* 14:92–98.

Sun, J. Y., X. S. Wu, and L. G. Wu. 2002. Single and multiple vesicle fusion induce different rates of endocytosis at a central synapse. *Nature*. 417:555–559.

Takagi, S., K. Obata, and H. Tsubokawa. 2002. GABAergic input contributes to activity-dependent change in cell volume in the hippocampal CA1 region. *Neurosci. Res.* 44:315–324.

Tao, L. J. 1999. Effects of osmotic stress on dextran diffusion in rat neocortex studied with integrative optical imaging. *Neurophysiology*. 81:2501–2507.

Wan, X., J. A. Harris and C. E. Morris. 1995. Responses of neurons to extreme osmomechanical stress. *J. Membr Biol.* 145:21–31.

Wu, S. Y., and J. E. Casida. 1996. Subacute neurotoxicity induced in mice by potent organophosphorus neuropathy target esterase inhibitors. *Toxicol. Appl. Pharmacol.* 139:195–202.

Xia, P., P. M. Bungay, C. C. Gibson, O. N. Kovbasnjuk, and K. R. Spring. 1998. Diffusion coefficients in the lateral intercellular spaces of Madin-Darby canine kidney cell epithelium determined with caged compounds. *Biophys. J.* 74:3302–3312.

Xu, J., D. Ziemnicka, J. Scalia, and L. Kotula. 2001. Monoclonal antibodies to alpha I spectrin Src homology 3 domain associate with macropinocytic vesicles in nonerythroid cells. *Brain Res.* 898:171–177.